*Desalination and Water Treatment*
www.deswater.com
doi: 10.1080/19443994.2013.833867

52 (2014) 7856–7865
December

Taylor & Francis
Taylor & Francis Group

# Optimization of ultrasonic synthesis of N-succinyl-chitosan and adsorption of $Zn^{2+}$ from aqueous solutions

Fang Li*, Chunmei Ding

*Department of Biochemical Engineering, Anhui Polytechnic University, Wuhu 241000, China*
*Tel. +86 18817517716; Fax: +86 64252151; email: zls9390@163.com*

Received 13 February 2013; Accepted 5 August 2013

ABSTRACT

N-succinyl-chitosan (N-NSC) was prepared by reacting chitosan (CS) with succinic anhydride (SA) under an ultrasonic radiation. The influences of three parameters (ultrasonic radiation power, mass ratio of SA to CS, and ultrasonic radiation time) on the degree of substitution (DS) of N-NSC were discussed and optimized with a response surface modeling. The optimum values of the above parameters for maximum value of DS were 118 W, 1.8:1, and 108 min, respectively. The adsorption performance of N-NSC for removing $Zn^{2+}$ from aqueous solution was investigated in a batch system. Kinetic experiments data of that adsorption of $Zn^{2+}$ onto N-NSC were fitted by pseudo-first-order, pseudo-second-order, and intraparticle diffusion kinetic models and the equilibrium isotherm data were described by six different isotherm equations. The adsorption follows pseudo-second-order kinetic model. The results demonstrate that the Langmuir equation is the best-fit model to describe the adsorption process with a maximum monolayer adsorption value of 135.41 mg/g, and Sips equation to predicit experimental value at an initial concentration of 100–700 mg/L, pH 5.0, and temperature 298 K.

*Keywords:* Chitosan; Succinylation; Ultrasonic radiation; Optimization; Adsorption; $Zn^{2+}$

## 1. Introduction

Chitosan (CS) obtained by the alkaline, partial deacetylation of chitin, is a natural copolymer of glucosamine and N-acetylglucosamine [1,2]. It is a non-toxic, biodegradable, biocompatible, and antibacterial material, which is regarded as a novel functional material and important renewable agricultural resource. In the last 20 years, chitosan has been spurred increasing an interest in water treatment as an adsorbent due to its low cost and biodegradation [3].

However, chitosan was hard to get for further application due to its property of low solubility in water. Many researches focused on the chemical modification of chitosan to improve its solubility in water. N-Succinyl-chitosan (N-NSC), which has many reactive functional groups such as amino group, carboxyl group, hydroxyl group, and so on, has attracted much attention for its good solubility in water. It has been extensively reported as a drug carrier, immobilizer, and expedients [4–6]. Also, there are some studies about the chelation ability of N-NSC with metal ions [7,8]. However, to our knowledge, there are still few reports about its adsorption capacity

*Corresponding author.

toward heavy metal ions in wastewater. Many physical and chemical properties of N-NSC such as solubility, swelling, and adsorption capacity are determined by degree of substitute (DS). Therefore, DS has been used as an important technical parameter for the study of chitosan or modified chitosan. Higher DS means better adsorption capacity for N-NSC [7]. In order to get an optimal value of DS of N-NSC, the experimental design and the optimization technique may have some advantages for the purpose [9–11].

The conventional preparation process of N-NSC usually requires long processing time owning to the low efficiency of mechanical stirring. Ultrasonic radiation can accelerate the reaction rate manifold than conventional one and has been successfully applied in the preparation of powdery chemical materials such as molecular sieve and zeolite [12,13].

Here, we reported the ultrasonic synthesis process of N-NSC, investigating three factors (ultrasonic radiation time, mass ratio of succinic anhydride (SA) and chitosan, and ultrasonic radiation power) that could affect to it, and building a mathematical model for the synthesis as a function of variables involved to find the reliable maximum value for DS using response surface methodology (RSM). N-NSC obtained in this study would be tested for its adsorption ability toward $Zn^{2+}$ ions. Also, the adsorption kinetics of $Zn^{2+}$ on N-NSC was studied. Furthermore, in order to understand the mechanism of the adsorption systems, six isotherms models were adopted to fit the isotherm data.

## 2. Experimental

### 2.1. Materials

Biochemical reagent grade chitosan (deacetylation degree > 92%) from Qindao Haiyang Co. Ltd (China) was used. All other chemicals were of reagent grade and were used without further purification. A stock zinc solution (1,400 mg/L) was prepared in distilled water with $ZnSO_4$. All working solutions were prepared by diluting these stock solutions with the distilled water. An ultrasonic generator, type YQ-120, with a frequency of 40 kHz was manufactured by Yijing Ultrasonic Cleaner Co. Ltd (China). The ultrasonic radiation power of the generator is optional from 30 to 300 W. IR spectra were recorded on a Shimadzu FT-IR spectrometer (IRPrestige-21). XRD spectra were determined by using a Bruker D8 powder diffraction meter with Cu Ka radiation in the range of 10–80°C at 40 kV and 30 mA. The results of DTA and TG were obtained with a Shimadzu DSC-60A equipment with the temperature range of 10–600°C and a heating rate of 20°C/min. SEM was examined by S4800 (Japan Hitachi corporation) at an accelerating voltage of 5 kV. The BET area of chitosan and N-NSC was performed using a Micromeritics ASAP 2010.

### 2.2. Ultrasonic radiation synthesis of N-NSC

Chitosan (0.640 g) was added to 100 mL aqueous 1% $CH_3OOH$ (v/v) with stirring and then transferred into a three-neck flask. SA was dissolved in acetone (20 mL) and added dropwise into the flask. The reaction mixture was then placed into an ultrasonic generator and was heated for a specific time under ultrasonic radiation. After cooling and filtering, the mixture was immersed in an hydrous ethanol for 12 h and was adjusted to the pH 10 by adding sodium hydroxide solution. Then, acetone was added to the solution and a white precipitate was formed. This precipitate was filtered and washed with 70% (w/v) of ethanol and 100% of acetone three times, respectively. Finally, the product was obtained by drying the precipitate at room temperature for 12 h.

### 2.3. Determination of degree of substitution

The degree of substitution of N-NSC was determined by using conductometric titration. The sample of 0.1 g N-NSC was dissolved in excess 0.1 mol/L HCl, and was titrated by 0.477 mol/L NaOH. The conductivity of the solution was detected using a conductivity meter digital model DDS-11A. All the titrations were done in quadruplicate. The degree of substitution (DS (%)) can be calculated from the equations below [14].

$$\mathrm{DS}/X = C_1V_1 - C_2V_2 \tag{1}$$

$$161X + 203Y + 262Z = m \tag{2}$$

$$(X + Z)/(X + Y + Z) = \mathrm{DD} \tag{3}$$

$$Z/(X + Y + Z) = \mathrm{DS} \tag{4}$$

where $C_1$ and $C_2$ refer to the concentration of standard solution of HCl and NaOH, respectively; $V_1$ is the volume of HCl, mL; $V_2$ is the volume of NaOH used in the titration corresponding to the inflection point in the conductivity graph (Fig. 1), mL; $X$ is the number of moles of nonsubstitution-acetylated unit with a molar molecular weight of 161; $Y$ is the number of moles of nonacetylated units with a molar molecular weight of 203; $Z$ is the number of succinyl unit with a

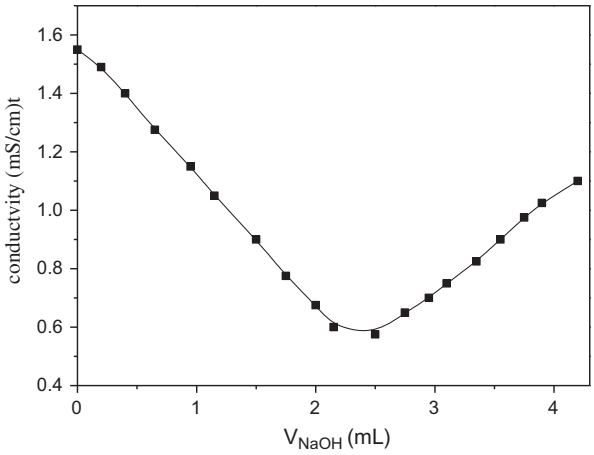


Fig. 1. Conductometric titration plot of the chitosan sample.

molar weight of 262; $m$ is the mass of the sample; DD is the degree of deacetylation of CS (DD = 92%); and DS the degree of substitution.

### 2.4. RSM design

RSM was used to optimize the synthesis conditions in order to obtain a high DS, and Box-Behnken design (BBD) was employed to design the experiments. Based on this method, with a minimum number of experiments, the interaction between the parameters and results could be analyzed. In this study, the effects of three independent variables, $x_1$ (mass ratio of SA and chitosan, m(SA)/m(CS)), $x_2$ (ultrasonic radiation time, $t$), and $x_3$ (ultrasonic radiation power, $P$), at three levels were investigated as listed in Table 1. Runs were performed at random. By the RSM, a quadratic polynomial equation was developed to predict the response as a function of independent variables involving their interactions, the response for the quadratic polynomial is described in Eq. (5). The adequacy of the model was justified through the analysis of variance (ANOVA).

$$Y = \beta_0 + \sum\sum \beta_i x_i + \sum \beta_{ii} x_i^2 + \sum\sum \beta_{ij} x_i x_j \quad (5)$$

Table 1
Experimental range and levels of independent variables

| Factors | Range and levels (coded) | | |
|---|---|---|---|
| | −1 | 0 | 1 |
| $m$(SA)/$m$(CS) ($x_1$) | 1 | 1.5 | 2 |
| $t$ ($x_2$, min) | 60 | 90 | 120 |
| $P$ ($x_3$, W) | 60 | 120 | 180 |

where $Y$ is the process response or output (dependent variable); $i$ and $j$ are the index numbers for the pattern; $\beta_0$ is the free or offset term called intercept term; $x_1$, $x_2$, and $x_i$ are the coded independent variables; $\beta_i$ is the first-order (linear) main effect; $\beta_{ii}$ is the squared effect; and $\beta_{ij}$ is the interaction effect.

### 2.5. Adsorption behavior toward $Zn^{2+}$

For the study of the effect of pH, 0.025 g N-NSC, and 50 mL of aqueous solution of 500 mg/L, zinc ions were added to a flask thermostatically maintained at 25°C for 6 h under magnetic stirring and the reaction mixtures were adjusted to different pH ranges. For kinetic studies, 50 mL of 400 mg/L $Zn^{2+}$ solution at pH 5 with 0.025 g N-NSC was agitated in a shaker at 25°C for a specified period of contact time. For adsorption isotherms, $Zn^{2+}$ solutions of different concentrations (100–700 mg/L) were agitated at 25°C with 0.025 g adsorbent and a fixed pH at 5 till the equilibrium was reached (10 h). Each experiment was replicated three times and the mean values were adopted. The amounts of the adsorbed metal ions were determined by spectrophotometer. The amount of metal ions adsorbed per gram of the N-NSC was calculated by Eq. (6).

$$q = V \times (C_0 - C_1)/m \quad (6)$$

where $q$ is the amount of heavy metal adsorbed onto the unit amount of N-NSC (mg/g); $C_0$ is the initial $Zn^{2+}$ ion concentration (mg/l); $C_1$ is the $Zn^{2+}$ ion concentrations at any time (mg/L); $V$ is the volume of the $Zn^{2+}$ ion solution (mL); and $m$ is the weight of the N-NSC (g).

### 2.6. Mathematical description

#### 2.6.1. Kinetic model

Pseudo-first-order, pseudo-second-order, and intraparticle diffusion equations (Eqs. (7)–(9)) are the most widely used equations in the adsorption process for the kinetic model [15,16].

$$\log(q_e - q_t) = \log q_e - \frac{k_1}{2.303} t \quad (7)$$

$$\frac{t}{q} = \frac{1}{k_2 q_e^2} + \frac{t}{q_e} \quad (8)$$

$$q_t = k_3 t^{0.5} \quad (9)$$

where $q_t$ and $q_e$ (mg/g) refer to the amount of adsorbed $Zn^{2+}$ at time $t$ and equilibrium time, respectively; $k_1$ is the rate constant of first-order adsorption ($min^{-1}$); $k_2$ is the rate constant of pseudo-second-order for the adsorption ($g\,mg^{-1}\,min^{-1}$); and. $k_3$ is intraparticle diffusion rate ($mg\,g^{-1}\,min^{0.5}$).

#### 2.6.2. Equilibrium isotherms

The Langmuir isotherms give a hypothesis of totally homogeneous adsorption sites on the surface of adsorbents. It is the most common isotherm modeling for adsorption process. In liner mathematical form, it is written as [17,18].

$$\frac{C_e}{q_e} = \frac{1}{q_m L} + \frac{C_e}{q_m} \tag{10}$$

where $q_m$ denotes the maximum adsorption capacity of the adsorbent (mg/g); $L$ denotes the Langmuir constant regarding the adsorption energy; and $C_e$ the denotes equilibrium concentration in mg/L.

The Freundlich isotherm is an empirical equation for a multilayer physical adsorption system. It assumes an exponential distribution of adsorption sites and energies. It describes the relationship between equilibrium liquid and solid phase capacity with a heterogeneous surface. It is represented in a linear form as [19].

$$\ln q_e = \ln K_f + n \ln C_e \tag{11}$$

where $K_f$ (mg/g) and $n$ are Freundlich constants and were obtained by calculating the slope and intercept of the Freundlich plots.

The Tempkin isotherm takes into account the effects of the heat of adsorption that decreases linearly with a coverage of the adsorbate and adsorbent interactions [4]. The Tempkin isotherm is represented by the following equation:

$$q_e = \frac{RT}{b_T}(\ln A) + \frac{RT}{b_T}(\ln C_e) \tag{12}$$

where $A$ (l/g) and $b_T$ (J/mol) are the Tempkin constants which can be determined from a plot of $q_e$ versus ln $C_e$.

The Sips isotherm model can be regarded as a combination of Langmuir and Freundlich equations and represented as Eq. (13) [20].

$$q_e = \frac{k_s C_e^{1/b}}{1 + \alpha_s C_e^{1/b}} \tag{13}$$

where $q_e$ is the total number of binding sites (mg/g); $b$ is the median association constant (mL/mg); and $1/b$ is the heterogeneity factor. If the value for $1/b$ is less than one, it indicates that the adsorbent possess heterogeneous sorption sites, while values closer to or even one indicate that the adsorbent has relatively more homogeneous ones.

The Redlich–Peterson (R–P) equation contains three parameters and incorporates the features of Langmuir and the Freundlich isotherms [21].

$$q_e = \frac{k_R C_e}{1 + \alpha_R C_e^{\beta}} \tag{14}$$

where $k_R$, $\alpha_R$, and $\beta$ are the R–P parameters; $\beta$ lies between 0 and 1, for $\beta$ equal to 1; and the R–P equation becomes a Langmuir form.

The Toth equation is used in heterogeneous systems, which assumes a quasi-Gaussian energy distribution, i.e. most sites have sorption energy lower than the peak of maximum sorption energy [22].

$$q_e = \frac{k_f C_e}{(a_t + C_e^t)^{1/t}} \tag{15}$$

where $k_f$, $\alpha_t$, and $t$ are the Toth parameters.

## 3. Results and discussion

### 3.1. Characterizations

#### 3.1.1. BET

According to $N_2$ adsorption and desorption isotherms, the surface area, pore diameter, and pore volume of chitosan and N-NSC are listed in Table 2. According to the International Union of Pure and Applied Chemistry (IUPAC) classifications, the pores of chitosan and N-NSC correspond to micropores ($2 < d < 50$ nm). Compared with chitosan, the BET surface area of N-NSC increases and the average pore diameter decreases, while the total pore volume does not change obviously.

#### 3.1.2. XRD

X-ray diffraction spectra were used to examine the crystal form of polymer. Fig. 2 shows the XRD patterns of chitosan (b) and N-NSC (a). From Fig. 2(b), two diffraction peaks can be observed at $2\theta = 11.6^\circ$ and $2\theta = 20^\circ$. Zhu et al. and co-workers reported that the reflection fall at $2\theta = 11.6^\circ$ corresponds to crystal form I and that the strongest reflection which appears at $2\theta = 20^\circ$ corresponds to crystal forms II [23].

Table 2
Physical characteristics of chitosan and N-NSC

| Adsorbent | $S_{BET}$ ($m^2/g$) | Langmuir surface area ($m^2/g$) | $D$ (nm) | Total pore volume ($cm^3/g$) |
|---|---|---|---|---|
| CS | 1.7 | 1.40 | 42.87 | 0.0054 |
| N-NCS | 3.6 | 3.56 | 12.56 | 0.0053 |

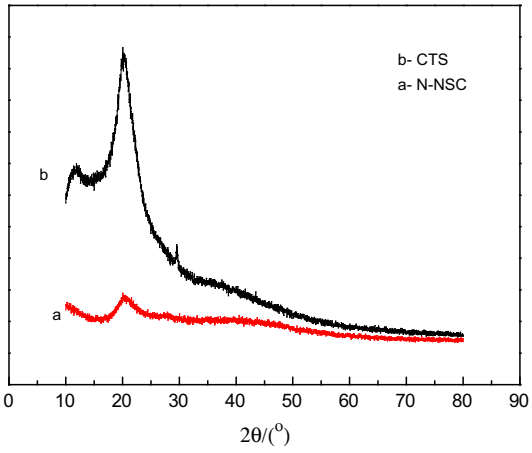


Fig. 2. XRD patterns of (a) N-NSC and (b) chitosan.

However, there is only one broad peak centerd at $2\theta = 20^\circ$ in the XRD spectrum of N-NSC (Fig. 2(a)). A very similar observation has been reported by Zhou et al. suggesting that hydrogen bonding capacity decreased greatly owing to the substitution of N-succinyl [24]. It is well known that chitosan cannot be dissolved in water. However, N-NSC in this study can be dissolved in distilled water to form a clear solution.

### 3.1.3. SEM

Fig. 3(a) represents pure chitosan. It presents a plate-like surface, smooth and nonporous. The morphology of N-NSC is shown in Fig. 3(b), where an irregular and porous structure was observed, indicating an increase of effective specific surface area and may provide more active sites to contact with $Zn^{2+}$.

### 3.1.4. TG and DTA analysis

The DTA/TG spectra of chitosan (Fig. 4(a)) and N-NSC (Fig. 4(b)) show some different information. For chitosan, there is one endothermic peak around 103.9℃ and two sharp exothermic peaks at 322.6 and 550℃, respectively. Combined with TG curve, the former endothermic peak may be owing to the loss of water. Two exothermic peaks are observed related to the thermal decomposition of chitsoan. There are also three corresponding peaks for N-NSC. However, these peaks are all at lower temperature compared to those of chitosan. It not only means a less stable for N-NSC, but also indicates that the structure of chitosan had been modified as a result of the introduction of succinyl group [24,25].

## 3.2. Optimization of reaction condition by RSM

Box–Behnken experimental design and corresponding results were presented in Table 3. The coefficient of the model for the response was estimated using multiple regression analysis technique embedded in the RSM. The quadratic model obtained was given as follows:

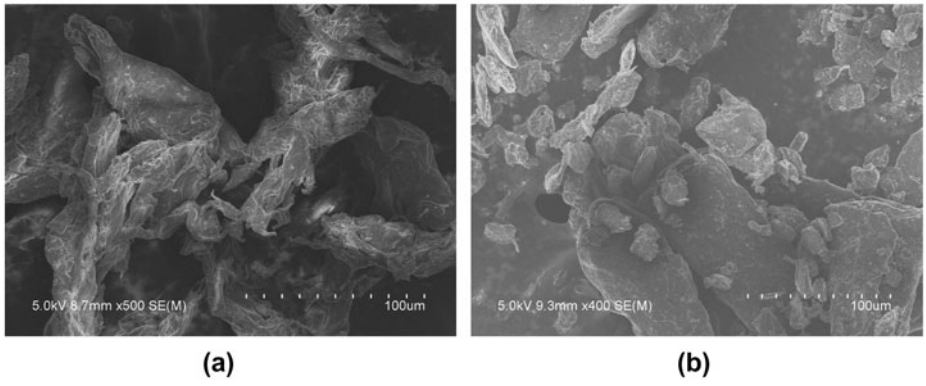


Fig. 3. SEM graph of chitosan (a) and N-NSC (b).

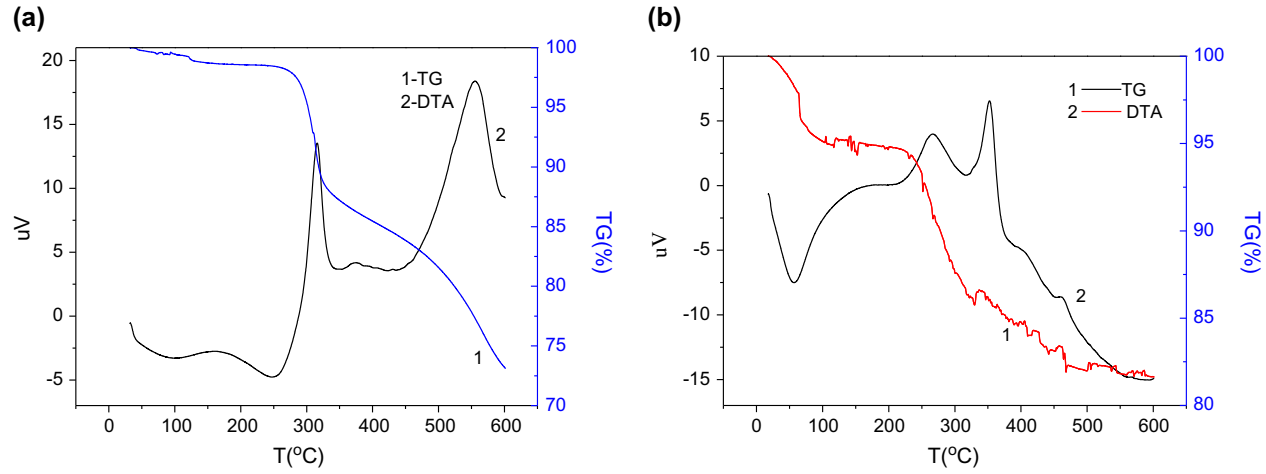


Fig. 4. TG and DTA curves for chitosan (a) and N-NSC (b).

Table 3
Box–Behnken experimental design for the three independent variables

| No. | $m$(SA)/$m$(CS) | React time ($t$) | Power ($P$) | Response (DS) | |
|---|---|---|---|---|---|
| | $x_1$ (uncoded) | $x_2$ (uncoded) | $x_3$ (uncoded) | Observed | Predicted |
| 1 | 1.5 | 60 | 60 | 0.18 | 0.211 |
| 2 | 2 | 90 | 120 | 0.69 | 0.825 |
| 3 | 1 | 60 | 60 | 0.48 | 0.454 |
| 4 | 1 | 120 | 180 | 0.58 | 0.509 |
| 5 | 1.5 | 60 | 60 | 0.67 | 0.654 |
| 6 | 2 | 90 | 120 | 0.32 | 0.317 |
| 7 | 1.5 | 90 | 120 | 0.65 | 0.65 |
| 8 | 1 | 90 | 120 | 0.53 | 0.572 |
| 9 | 1.5 | 120 | 180 | 0.78 | 0.699 |
| 10 | 1.5 | 90 | 120 | 0.65 | 0.65 |
| 11 | 2 | 60 | 60 | 0.62 | 0.631 |
| 12 | 1.5 | 90 | 120 | 0.65 | 0.65 |
| 13 | 1.5 | 90 | 120 | 0.65 | 0.65 |
| 14 | 1 | 90 | 120 | 0.22 | 0.215 |
| 15 | 1.5 | 90 | 120 | 0.65 | 0.65 |
| 16 | 1.5 | 120 | 180 | 0.32 | 0.276 |
| 17 | 2 | 120 | 180 | 0.66 | 0.686 |

$$DS = 0.65 + 0.065x_1 + 0.20x_2 + 0.041x_3 + 0.015x_1x_2 - 0.005x_1x_3 - 0.013x_2x_3 - 0.059x_1^2 - 0.15x_2^2 - 0.016x_3^2 \quad (16)$$

The effects and significance of the variables in the ultrasonic syntheses were evaluated using Pareto's charts. The length of each bar is proportional to the absolute value of its associated regression coefficients or estimated effect. The effects of all parameters, interactions as well as quadratic terms, are standardized (each effect is divided by its standard error). The order in which the bars are displayed corresponds to the order of the size of the effect. From Fig. 5, we can see the significance of the three factors in the order of $x_2 > x_1 > x_3$.

The results of ANOVA for Eq. (16) were given in Table 4. The larger the value of $F$ and smaller the value of $P$, the more significant is the corresponding coefficient term [26]. By analyzing the $F$ and $P$ values from Table 4, it was found that the $x_2$ has high significance, and $x_1$ and $x_3$ terms have moderate significance; the other terms are insignificant in the

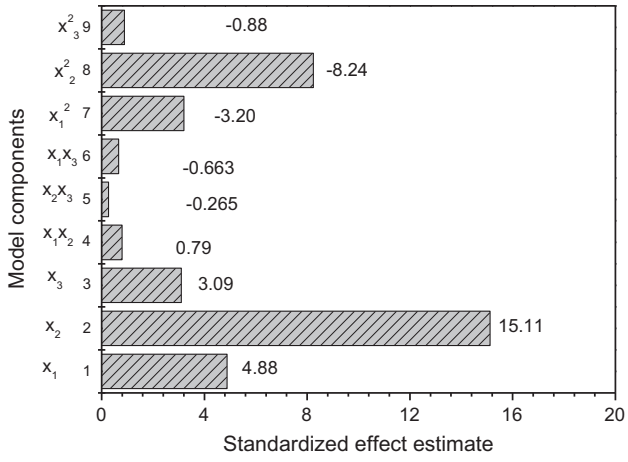


Fig. 5. Pareto's chart (absolute value).

equation and are not required to explain the synthesis process. Therefore, the model was reduced to the following form by neglecting insignificant terms.

$$DS(\%) = 0.65 + 0.065x_1 + 0.20x_2 + 0.041x_3 + 0.015x_1x_2 - 0.059x_1^2 - 0.15x_2^2 \quad (17)$$

3D response surfaces plot was given in Fig. 6. Also, the optimum value of DS was obtained according to the software optimization step, namely, the desired goal for each parameter (m(SA)/m(CS), reaction time, and power) was chosen "within the range," while the response (DS) was defined as "maximum." The confirmation experiments were carried out under optimized conditions. The results given by model and experiments are listed in Table 5, and the similar value of DS verifies the accuracy of the optimum conditions obtained from BBD experiments.

### 3.3. Adsorption study toward $Zn^{2+}$

#### 3.3.1. Effect of pH

The effect of pH on the adsorption process has been investigated over the range from 2.0 to 7.0. As indicated in Fig. 7, the maximum capacity of $Zn^{2+}$ adsorption occurred at pH 5.0. The reduced uptake of $Zn^{2+}$ after 5.0 can be explained as the formation of metal hydroxide species such as soluble $Zn^{2+}$ and/or insoluble precipitate of $Zn(OH)_2$.

#### 3.3.2. Adsorption kinetics

Fig. 8 indicated the effect of contact time on adsorption at different temperatures. It can be observed that adsorption of $Zn^{2+}$ was rapid firstly, then slowly increased with increasing time and finally attained equilibrium at about 4 h. This can be explained by the three stages of mechanism for metal ion adsorption on porous adsorbents: in the first stage, $Zn^{2+}$ adsorption is mainly carried out on the external surface of adsorbent; the second stage corresponds to diffusion of ions into the pores of adsorbent in which diffusion resistance increases, causing a decrease in the adsorption rate; and the last stage ascribes to the adsorption of the ions on the internal surface of adsorbent in which concentration-driving force becomes more and more small and adsorption has been basically achieved balance. The experimental data of kinetics (Fig. 8) were analyzed using a pseudo-first-order equation (Eq. (7)), pseudo-second-order equation (Eq. (8)), and the intraparticle diffusion model (Eq. (9)).

Correlation coefficient of 0.8886, 0.9982, and 0.8438 was obtained from linear fit of $\log(q_e - q_t)$ and $t$, $t/q_t$ and

Table 4
ANOVA for second-order model

| Source | Sum of squares | $d_f$ | Mean square | $F$ value | $p$-value Prob > F |
|---|---|---|---|---|---|
| model | 0.4914 | 9 | 0.05461 | 38.51 | <0.0001 |
| $x_1$ | 0.0338 | 1 | 0.0338 | 23.83 | 0.0018 |
| $x_2$ | 0.3240 | 1 | 0.3240 | 228.52 | <0.0001 |
| $x_3$ | 0.01361 | 1 | 0.01361 | 9.601 | 0.0174 |
| $x_1 \times x_2$ | 0.0009 | 1 | 0.0009 | 0.6347 | 0.059 |
| $x_1 \times x_3$ | 0.0001 | 1 | 0.0001 | 0.0705 | 0.7982 |
| $x_2 \times x_3$ | 0.000625 | 1 | 0.000625 | 0.4408 | 0.5280 |
| $x_1^2$ | 0.01453 | 1 | 0.01453 | 10.25 | 0.0150 |
| $x_2^2$ | 0.09632 | 1 | 0.09632 | 67.93 | <0.0001 |
| $x_3^2$ | 0.001112 | 1 | 0.001112 | 0.7841 | 0.4053 |
| Residual | 0.009925 | 7 | 0.001418 | | |
| Lack of fit | 0.009925 | 3 | 0.003308 | | |
| Pure error | 0 | 4 | 0 | | |

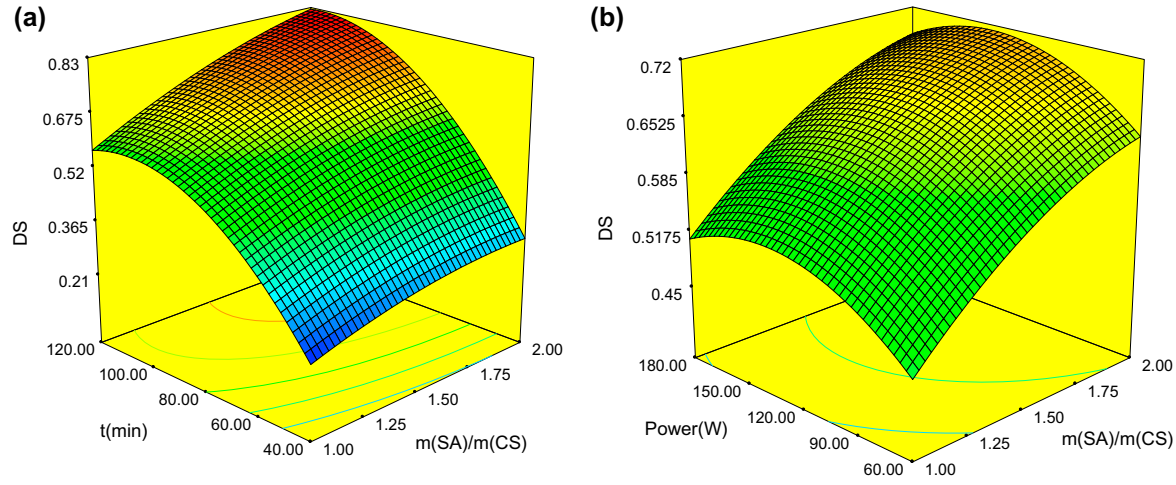


Fig. 6. 3D response surfaces plot.

Table 5
Optimal synthesis conditions from the model

| Parameters | $m$ (SA)/$m$ (CS) | $t$ (min) | Power (W) | Response (DS) |
|---|---|---|---|---|
| Parameter given by model | 1.8 | 106.3 | 118 | 0.75 |
| Actual results obtained after confirmation experiments | 1.8 | 108 | 118 | 0.76 |

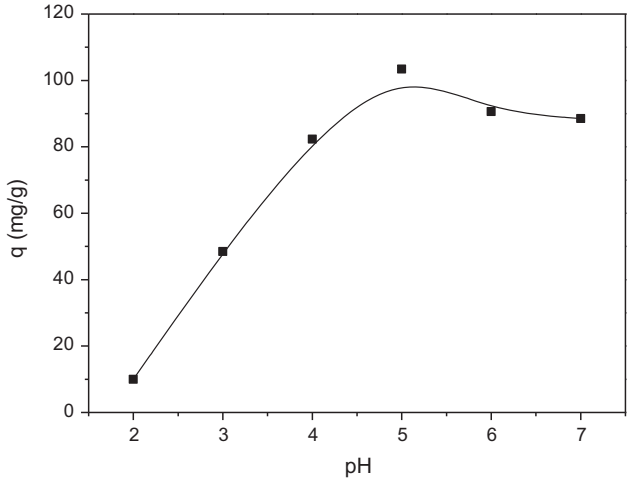


Fig. 7. Effect of pH on $Zn^{2+}$ adsorption.

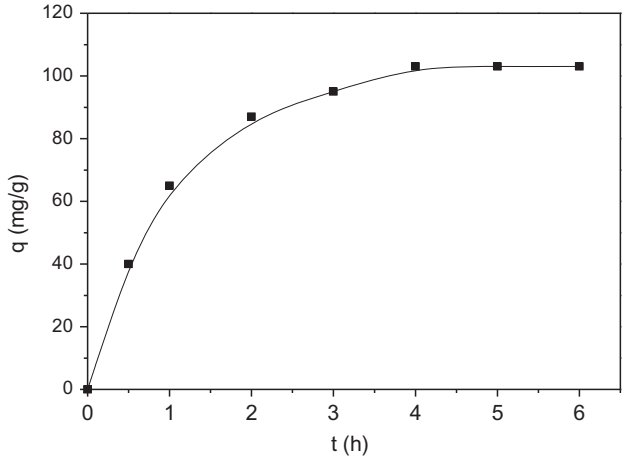


Fig. 8. Kinetics of $Zn^{2+}$ adsorption on N-NSC.

$t$, and $q_t$ and $t^{0.5}$ for Eqs. (7)–(9), respectively. It indicates $Zn^{2+}$ adsorption on the N-NSC obeys pseudo-second-order kinetic model. Pseudo-second-order kinetic model assumes that the rate-limiting step may be chemical adsorption [28].

### 3.3.3. Equilibrium isotherms

The equilibrium adsorption isotherms are the most important information to understand the mechanism of the adsorption systems. In order to optimize the design of an adsorption system to remove the metal, it is important to establish the most appropriate correlation of the equilibrium data. Fig. 9 shows isotherms at different temperatures for a specific system [28]. It can be seen that adsorption capacity increased with temperature, indicating that the adsorption of $Zn^{2+}$ is endothermic. Here, six isotherm equations (Eqs. (10)–(15)) were used to correlate equilibrium data at 298 K. The two parameters of the Langmuir, Freundlich, and Temkin models could be

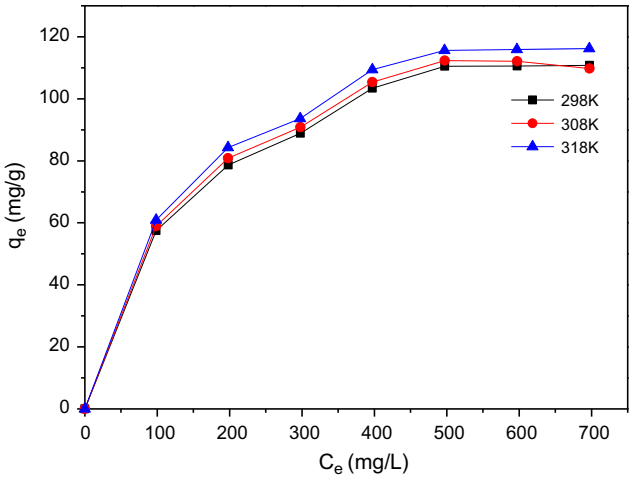


Fig. 9. Equilibrium adsorption isotherms for $Zn^{2+}$-N-NSC system at different temperatures.

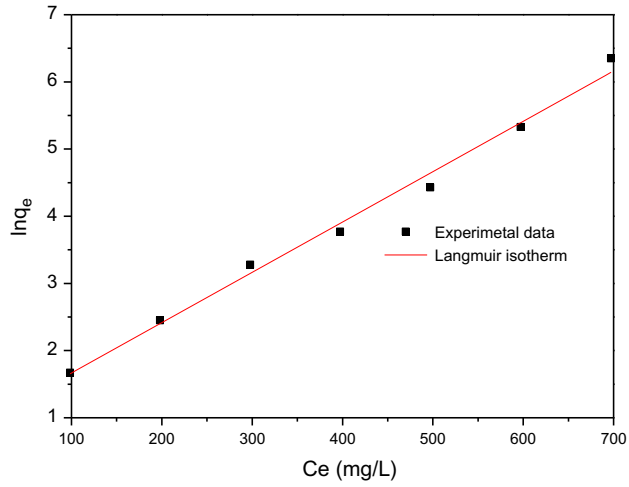


Fig. 10. Langmuir plot for the adsorption of $Zn^{2+}$ onto N-NSC.

obtained by linear regression analysis. For the other models, the parameters were estimated by nonlinear fit. The obtained constants were shown in Tables 6 and 7, respectively.

The values of correlation coefficient ($R^2$), a measure of the goodness of fitting, confirm that the Langmuir, Sips, RP, Toth, and Tempkin models result in closer prediction of the isotherms compared with the experimental data. The other two parameter models of the Freundlich showed a relatively poor fit of the experimental data. On the basis of the $R^2$ values, the order of linear best-fit was Langmuir model > Sips model > Redlich–Peterson model > Tempkin model > Freundlich model > Toth model at 298 K.

The maximum adsorption capacity at 298 K calculated from the Langmuir isotherm and Sips isotherm was 135.41 and 118.3 mg/g, respectively. This indicates that Sips model can be used to predicit experimental value more precisely than Langmuir especially at a high concentration of adsorbate [21]. The values of Sips model exponent b were less than one but closer to one indicates that this model behaves more Langmuir than Freundlich and adsorbent has relatively more homogeneous binding sites. Besides, the value of $\beta$ in R-P model was closer to unity implying that the isotherms was more approaching the Langmuir than the Freundlich model. Fig. 10 shows that the equilibrium data in this study were fitted well with Langmuir isotherm model with $R^2 = 0.997$. In conclusion, Langmuir or Sips model can be used to correlate experimental data. For the equilibrium study, Fan et al. [29] studied the adsorption of $Zn^{2+}$ by cross-linked magnetic-modified chitosan. They reported that the equilibrium data at different temperatures were fitted well with Langmuir isotherms. Ding et al. [30] investigated the adsorption of $Zn^{2+}$ onto modified chitosan. The results also indicated Langmuir isotherms fitted the equilibrium data best. According to Chen et al. [31], the results obtained from the equilibrium isotherms adsorption studies of $Zn^{2+}$ ions being analyzed in three adsorption models also well fitted to the Langmuir isotherm equation than the other two isotherm equations.

Table 6
Isotherm constants for adsorption models with two parameters at 298 K

| Langmuir | | | | Freundlich | | | Tempkin isotherm | | |
|---|---|---|---|---|---|---|---|---|---|
| $q_m$ | $L$ | $R_L$ | $R^2$ | $n$ | $k_f$ | $R^2$ | $b_t$ | $A$ | $R^2$ |
| 135.31 | 0.0074 | 0.161 | 0.997 | 0.35 | 11.99 | 0.956 | 84.58 | 0.406 | 0.931 |

Table 7
Isotherm constants for adsorption models with three parameters at 298 K

| Redlich-Peterson | | | | Sips | | | | Toth | | | |
|---|---|---|---|---|---|---|---|---|---|---|---|
| $k$ | $\alpha_R$ | $\beta$ | $R^2$ | $\alpha_s$ | $b$ | $k_s$ | $R^2$ | $k_t$ | $\alpha_r$ | $t$ | $R^2$ |
| 1.247 | 0.01495 | 0.944 | 0.989 | 0.915 | 0.914 | 108.32 | 0.993 | 222.61 | 225.12 | 1.09 | 0.9604 |

## 4. Conclusions

In this research, RSM was used to the optimization of synthesis of N-NSC by ultrasonic radiation. The development of a mathematical model for synthesis process appears to be a useful tool for predication and understanding of the interaction effects between the experimental parameters. The optimum reaction conditions were as follows: ultrasonic radiation time, 108 min; mass ratio of SA to chitosan, 1.8:1; ultrasonic radiation power, 118 W; and reaction time, 108 min. The obtained value of the degree of substitution of N-NSC is above 0.75. Adsorption capacity of N-NSC toward a high concentration of $Zn^{2+}$ from aqueous solution was studied. The results showed that maximum adsorption capacity of N-NSC based on Langmuir isotherms model at 298 K was 135.31 mg/g. However, the percentage of removal is low as a result of low adsorbent dosage and high concentration of $Zn^{2+}$ used. $Zn^{2+}$ adsorption onto N-NSC is found to be pH-dependent, and follows the pseudo-second-order kinetic model and Langmuir and Sips isotherm equations.

## Acknowledgments

The authors gratefully acknowledge the financial support provided by the Natural Science Foundation of Anhui province (KJ2011B105).

## References

[1] L. Wang, A.Q. Wang, Adsorption properties of congo red from aqueous solution onto N, O-carboxymethyl-chitosan, Bioresource. Technol. 99 (2008) 1403–1408.
[2] W.S. Wan Ngah, L.C. Teong, M.A.K.M. Hanafiah, Adsorption of dyes and heavy metal ions by chitosan composites: A review, Carbohyd. Polym. 83 (2011) 1446–1456.
[3] A. Shafaei, F.Z. Ashtiani, T. Kaghazchi, Equilibrium studies of the sorption of Hg(II) ions onto chitosan, Chem. Eng. J. 133 (2007) 311–316.
[4] J.S. Piccin, M.L.G. Vieira, J.O. Gonçalves, G.L. Dotto, L.A.A. Pinto, Adsorption of FD&C red no. 40 by chitosan: Isotherms analysis, J. Food. Eng. 95 (2009) 16–20.
[5] Y. Kato, H. Onishi, Y. Machida, Evaluation of N-succinyl-chitosan as a systemic long-circulating polymer, Biomaterials 21 (2000) 1579–1585.
[6] Y. Kato, H. Onishi, Y. Machida, N-succinyl-chitosan as a drug carrier: water-insoluble and water-soluble conjugates, Biomaterials 25 (2004) 907–915.
[7] S.L. Sun, A.Q. Wang, Adsorption properties of N-succinyl-chitosan and cross-linked N-succinyl-chitosan resin with Pb (II) as template ions, Sep. Purif. Technol. 51 (2006) 409–415.
[8] S.L. Sun, A.Q. Wang, Adsorption kinetics of Cu(II) ions using N, O-carboxymethyl-chitosan, J. Hazard. Mater. 131 (2006) 103–111.
[9] K. Ravikumar, K. Pakshirajan, T. Swaminathan, K. Balu, Optimization of batch process parameters using response surface methodology for dye removal by a novel adsorbent, Chem. Eng. J. 105 (2005) 131–138.
[10] K. Yetilmezsoy, S. Demirel, R.J. Vanderbe, Response surface modeling of Pb(II) removal from aqueous solution by Pistacia vera L.: Box–Behnken experimental design, J. Hazard. Mater. 171 (2009) 551–562.
[11] N. SahuJ, J. Acharya, B.C. Meikap, Response surface modeling and optimization of chromium (VI) removal from aqueous solution using Tamarind wood activated carbon in batch process, J. Hazard. Mater. 172 (2009) 818–825.
[12] M.T. Run, S.Z. Wu, G. Wu, Ultrasonic synthesis of mesoporous molecular sieve, Micropor. Mesopor. Mat. 74 (2004) 37–47.
[13] C. Belviso, F. Cavalcante, A. Lettino, S. Fiore, Effects of ultrasonic treatment on zeolite synthesized from coal fly ash, Ultrason. Sonochem. 18 (2011) 661–668.
[14] L. Raymond, F.G. Morin, R.H. Marchessault, Degree of deacetylation of chitosan using conductometric titration and solid-state NMR, Carbohydr. Res. 246 (1993) 331–336.
[15] E. Demirbas, M.Z. Nas, Batch kinetic and equilibrium studies of adsorption of Reactive Blue 21 by fly ash and sepiolite, Desalination 243 (2008) 243–256.
[16] Y.S. Ho, Review of second-order models for adsorption systems, J. Hazard. Mater. 136 (2006) 681–689.
[17] N.M. Mahmoodi, R. Salehi, M. Arami, H. Bahrami, Dye removal from colored textile wastewater using chitosan in binary systems, Desalination 267 (2011) 64–72.
[18] M.R. Gandhi, G.N. Kousaly, N. Viswanathan, S. Meenakshi, Sorption behaviour of copper on chemically modified chitosan beads from aqueous solution, Carbohyd. Polym 83 (2011) 1082–1087.
[19] Ö. Tunc, H. Tanacı, Z. Aksu, Potential use of cotton plant wastes for the removal of Remazol Black B reactive dye, J. Hazard. Mat. 163 (2009) 187–198.
[20] K.Y. Foo, B.H. Hameed, Insights into the modeling of adsorption isotherm systems [J], Chem. Eng. J. 156 (2010) 2–10.
[21] Y.W. Chen, W.J. Long, Preparation and characterization of magnetic chitosan nanoparticles and its application for Cu(II) removal, Chem. Eng. J. 168 (2011) 286–292.
[22] J. Febriant, A.N. Kosasih, J. Sunarso, Y.-H. Ju, N. Indraswati, S. Ismadji, Equilibrium and kinetic studies in adsorption of heavy metals using biosorbent: A summary of recent studies, J. Hazard. Mat. 162 (2009) 616–645.
[23] R.J. Samuels, Solid state characterization of the structure of chitosan films, J. Polym. Sci. B. 19 (1981) 1081–1105.
[24] J.Q. Zhou, J.W. Wang, Immobilization of alliinase with a water soluble-insoluble reversible N-succinyl-chitosan for allicin production, Enzyme Micro. Tech. 45 (2009) 299–304.
[25] A.P. Zhu, T. Chen, L.H. Yuan, H. Wu, P. Lu, Synthesis and characterization of N-succinyl-chitosan and its self-assembly of nanospheres, Carbohyd. Polym. 66 (2006) 274–279.
[26] K. Bahadir, K. Orbahti, M.A. Rauf, Application of response surface analysis to the photolytic degradation of basic red 2 dye, Chem. Eng. J. 138 (2008) 166–171.
[27] F.C. Wu, R.L. Tseng, R.S. Juang, Kinetic modeling of liquid-phase adsorption of reactive dyes and metal ions on chitosan, Water Res. 35 (2001) 613–618.
[28] Z. Yian, A.Q. Wang, Removal of heavy metals using polyvinyl alcohol semi-IPN poly(acrylic acid)/tourmaline composite optimized with response surface methodology, Chem. Eng. J. 162 (2010) 1–8.
[29] L.L. Fan, C.N. Luo, Z. Lv, F. Lu, H.M. Qiu, Preparation of magnetic modified chitosan and adsorption of $Zn^{2+}$ from aqueous Solutions, Colloid Surf., B 88 (2011) 574–581.
[30] P. Ding, K.L. Huang, G.Y. Li, W.W. Zeng, Mechanisms and kinetics of chelating reaction between novel chitosan derivatives and Zn(II), J. Hazard. Mat. 146 (2007) 58–64.
[31] A.H. Chen, S.C. Liu, C.Y. Chen, C.Y. Chen, Comparative adsorption of Cu (II), Zn (II), and Pb (II) ions in aqueous solution on the crosslinked chitosan with epichlorohydrin, J. Hazard. Mat. 154 (2008) 184–191.